Check for updates

Investigation of Gallium–Boron Spin-On Codoping for poly-Si/SiO_x Passivating Contacts

Thien N. Truong, Tien T. Le, Di Yan, Sieu Pheng Phang, Mike Tebyetekerwa, Matthew Young, Mowafak Al-Jassim, Andres Cuevas, Daniel Macdonald, Josua Stuckelberger,* and Hieu T. Nguyen**

A doping technique for p-type poly-Si/SiOx passivating contacts using a spin-on method for different mixtures of Ga and B glass solutions is presented. Effects of solution mixing ratios on the contact performance (implied open circuit voltage iV_{oc}, contact resistivity ρ_c) are investigated. For all as-annealed samples at different drive-in temperatures, increasing the percentage of Ga in the solution shows a decrement in iV_{oc} (from ~680 to ~610 mV) and increment in ρ_c (from ~3 to ~800 mΩ cm^2). After a hydrogenation treatment by depositing a SiN_x/AlO_x stack followed by forming gas annealing, all samples show improved iVoc (~700 mV with Ga-B co-doped, and ~720 mV with all Ga). Interestingly, when co-doping Ga with B, even a small amount of B in the mixing solution shows negative effects on the surface passivation. Active and total dopant profiles obtained by electrical capacitance voltage and secondary-ion mass spectrometry measurements, respectively, reveal a relatively low percentage of electrically-active Ga and B in the poly-Si and Si layers. These results help understand the different features of the two dopants: a low ρ_c with B, a good passivation with Ga, their degree of activation inside the poly-Si and Si layers, and the annealing effects.

1. Introduction

Passivating contacts based on doped polycrystalline silicon (poly-Si) on interfacial oxide (SiO_x) (referred to here as poly-Si/SiO_x stacks) are a well-known technology for high-efficiency Si solar cells, with many groups reporting conversion efficiencies of over 25%.[1–5] Recently, industrial production of large-area screen-printed solar cells incorporating the passivating contacts has shown efficiencies over 25.2%,[6] demonstrating their compatibility with current industrial high-temperature dopant diffusion and metallization processes. Common approaches for doping the poly-Si layer can be broadly categorized into two main groups: in situ and ex situ. In the in situ methods, both the dopant element and the silicon are deposited simultaneously, the former then being activated by annealing in an inert environment at a high temperature.[7–15] Meanwhile, in the ex situ methods, an intrinsic Si film is formed before being doped.[16–24] Common ex situ doping methods used in Si solar cell manufacturing include gas diffusion, ion implantation, and liquid-based doping.[25] Among them, spin-on doping is currently attracting interest from the photovoltaic research community due to its convenience and simplicity.[26,27] The source of dopants for the spin-on process is a solution of dopant-containing silicate glass in alcohol. This glass solution can be easily spun onto the Si wafer at room temperature. For higher throughput, such as in an industrial manufacturing line, the solution can potentially be sprayed,[25] tape cast,[28] spin-coated,[27] or inkjet-printed.[29] In addition, this spin-on doping method brings the benefit of using less toxic precursors compared with conventional gas diffusion or ion implantation processes.[30,31]

Of the p-type dopant sources for the spin-on method, boron (B) and gallium (Ga) glass solutions are the most common ones. Boron has a smaller atomic radius than Si (0.088 nm vs 0.117 nm, respectively). Meanwhile, the atomic radius of Ga is larger than that of Si (0.126 nm). The difference in radius leads to a difference in lattice strain when the dopants diffuse into the Si crystal.[32–34] Therefore, the formation of defects and gettering effects in the two doped Si films could be different. Previous work on lab-scale Ga doping (by ion implantation and spin-on

T. N. Truong, T. T. Le, S. P. Phang, A. Cuevas, D. Macdonald, J. Stuckelberger, H. T. Nguyen
School of Engineering
The Australian National University
Canberra, ACT 2601, Australia
E-mail: thien.truong@anu.edu.au; josua.stuckelberger@anu.edu.au; hieu.nguyen@anu.edu.au

D. Yan
Department of Electrical and Electronic Engineering
The University of Melbourne
Victoria 3010, Australia

M. Tebyetekerwa
School of Mechanical, Medical and Process Engineering
Queensland University of Technology
Brisbane, QLD 4000, Australia

M. Young, M. Al-Jassim
National Renewable Energy Laboratory
Golden, CO 80401, USA

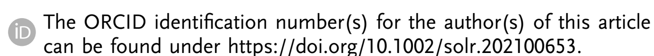
The ORCID identification number(s) for the author(s) of this article can be found under https://doi.org/10.1002/solr.202100653.

DOI: 10.1002/solr.202100653

© 2021 Wiley-VCH GmbH

2367198x, 2021, 12, Downloaded from https://onlinelibrary.wiley.com/doi/10.1002/solr.202100653 by The Australian National Univer, Wiley Online Library on [31/01/2023]. See the Terms and Conditions (https://onlinelibrary.wiley.com/terms-and-conditions) on Wiley Online Library for rules of use; OA articles are governed by the applicable Creative Commons License

2367198x, 2021, 12, Downloaded from https://onlinelibrary.wiley.com/doi/10.1002/solr.202100653 by The Australian National Univer, Wiley Online Library on [31/01/2023]. See the Terms and Conditions (https://onlinelibrary.wiley.com/terms-and-conditions) on Wiley Online Library for rules of use; OA articles are governed by the applicable Creative Commons License

doping) of poly-Si layers has shown an excellent performance in passivation (iV_{oc} ≈735 mV) but, once metallized, the doped Si films had a very high contact resistivity.[34] Meanwhile, with spin-on doping of poly-Si layers with B using industrial tools, a relatively high performance (iV_{oc} ≈720 mV) in combination with a low contact resistivity ($\rho_c < 5$ mΩ cm^2) can be achieved.[26] The high contact resistance in the case of Ga doping was explained by two possible theories: difficulties while etching of the poly-Si films due to an oxide layer formed on the surface, or Ga dopants being depleted at the surface or not activated.[34] In fact, active and total doping profiles obtained by electrochemical capacitance–voltage (ECV) and secondary ion mass spectrometry (SIMS) measurements in our work will show that the latter is more likely. Generally, the doping of Ga often requires a high-temperature annealing step to drive the dopants[34–36] also, it is known that the diffusion of Ga in SiO_x is faster than in c-Si.[37] Therefore, the Ga atoms are unlikely to pileup at or breakup the SiO_x interface. Meanwhile, the amount of Ga in the poly-Si film will likely be lower than in the B case due to the lower solid solubility of Ga in Si.[38]

To overcome the disadvantage of a high contact resistivity Ga doping with and to understand better its underlying mechanisms, in this work we vary the volume percentage of Ga and B in a mixed Ga + B solution to investigate the performance and electrical properties of Ga + B codoped poly-Si/SiO_x passivating contacts. By combining various characterization techniques such as photoconductance decay, ECV, and SIMS, we examine the change in the optoelectronic properties and diffusion behaviors of B and Ga into the poly-Si/SiO_x/c-Si substrate. From the results, we demonstrate that the codoping of Ga and B might be an alternative route to fabricate p-type poly-Si passivating contacts with both low contact resistivity and low surface recombination.

2. Experimental Section

The experimental processes are graphically shown in **Figure 1**. Gallium-doped p-type (100)-oriented Czochralski (Cz) wafers with a base resistivity of 0.4–1.1 Ω cm and a thickness of 175 μm were used for all experiments. After a saw damage etching step in a tetramethylammonium hydroxide (TMAH) solution and a standard radio corporation of america (RCA) cleaning step, a thermal oxidation process at 600 °C for 5 min was performed in pure oxygen to form an ultrathin (<2 nm) silicon oxide (SiO_x) layer on both sides of the substrate. Subsequently, intrinsic poly-Si layers with a thickness of ≈80 nm were deposited on top of the oxide film using a low-pressure chemical vapor deposition (LPCVD) system. The deposition was performed at 520 °C and a pressure of 300 mTorr for a duration of 80 min. The resultant poly-Si layer had an average thickness of ≈80 nm, as measured by an ellipsometer (J.A. Woollam ESM-300) using focusing probes. Then, the samples were cleaned by the standard RCA procedure and a dopant containing spin-on glass solution was spin-coated on both sides of these substrates using a spin coater (Laurell WS-650-23NPPB). The spin-on glass solution was varied between boron only (B-1500, [B] ≈7.2×10^{21} cm^{-3}), gallium only (Ga-100, [Ga] ≈4×10^{21} cm^{-3}, from Desert Silicon), and a gallium–boron (Ga + B) mixture with different volume percentages. The samples were then soft-baked at 90 °C for 10 min in a furnace, and hard-baked at 200 °C for 6 min on a hot plate. For the mixtures of Ga and B, different volume percentages of a total of 6 mL solution were chosen (e.g., 25, 50, 75% volume of Ga solution in Ga + B solution). We assume here that the glass film after baking behaves as an infinite source of dopants. Next, to drive the dopants into the poly-Si films and the underlying wafer, an annealing step with N_2 in a quartz tube furnace was performed at various temperatures from 900 to 1000 °C for 60 min. Subsequently, the silica glass layers were removed by dipping the samples in a dilute 3% hydrofluoric acid (HF) solution. Finally, the samples were hydrogenated by depositing a ≈20 nm AlO_x layer by thermal-assisted atomic layer deposition (ALD), covered by a ≈50 nm SiN_x layer by plasma-enhanced chemical vapor deposition (PECVD), and subsequently annealing them in forming gas (FGA, 5% H_2, 95% Ar) at 425 °C for 30 min. For contact resistivity measurements with the Cox and Strack method,[39] another

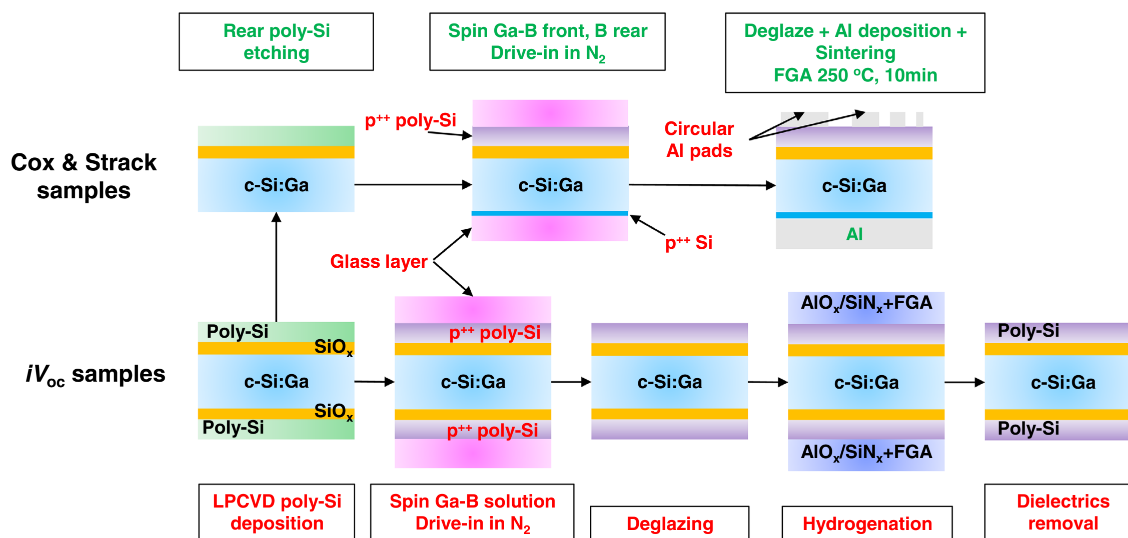

Figure 1. Details of the experimental processes.

© 2021 Wiley-VCH GmbH

2367198x, 2021, 12, Downloaded from https://onlinelibrary.wiley.com/doi/10.1002/solr.202100653 by The Australian National Univer, Wiley Online Library on [31/01/2023]. See the Terms and Conditions (https://onlinelibrary.wiley.com/terms-and-conditions) on Wiley Online Library for rules of use; OA articles are governed by the applicable Creative Commons License

set of samples went through the same processes described earlier, except the rear poly-Si layers were removed and those surfaces were spin-coated with a B glass film only. This is to create an identical heavy diffused p^{++} layer for the rear full area contacts of all samples. After the spin coating and drive-in steps, the samples were deglazed and 300 nm Al films were deposited on the front and rear sides of the samples using thermal evaporation. The front Al contact patterns were formed by a shadow mask with circles having different diameters. Finally, the samples were sintered in the forming gas at 250 °C for 10 min before the contact resistivity measurements.

A Sinton WCT-120 lifetime tester based on the photoconductance decay (PCD) method in transient mode was used to measure the resulting implied open-circuit voltage (iV_{oc}) values at 1 sun before and after the hydrogenation process (AlO_x/SiN_x + FGA). The electrically active dopant profiles were measured by an ECV setup (WEP Wafer Profiler CVP21). The total dopant profiles of Ga and B were obtained by a Cameca IMS 7f dynamic SIMS system using Cs+ primary ion at 10 kV with the sample at a −5 kV potential for negative secondary ions and an impact energy of 15 kV.

3. Results and Discussion

First, we investigate the effects of different volume percentages of Ga solution in the Ga + B mixed solution on the performance of the poly-Si/SiO_x passivating contacts annealed at various drive-in temperatures. The implied open-circuit voltage (iV_{oc}) and contact resistivity (ρ_c) represent the performance of the passivating contacts. Four different drive-in temperatures (900–1000 °C) with a fixed annealing time of 60 min were used. **Figure 2**A shows the iV_{oc} as a function of the Ga volume percentage in the Ga + B solution, before (open symbols, dashed lines) and after a hydrogenation treatment by FGA annealing of AlO_x/SiN_x stacks (filled symbols, solid lines). As can be seen from Figure 2A, before hydrogenation all the samples show a decreasing iV_{oc} with increasing Ga volume percentage in the solution, although each volume percentage has an optimum annealing temperature. Notably, for all samples spin-coated with 100% Ga solution, the iV_{oc} drops to a very low value (≈610 mV), irrespective of the diffusion temperature. This low iV_{oc} is likely due to a very low level of active dopants in the poly-Si film, as will be shown later in the corresponding ECV dopant profiles. When being codoped with B, there is an increase in the active doping level inside the films, leading to a better performance. It is worth noting here that, at the as-diffused, prehydrogenation state, the defect density at the interface is relatively high, especially for p+-doped surfaces.[40] In this state doping the shallow region underneath the oxide interface is normally a useful tool for reducing recombination (i.e., improving passivation) because it creates a strong imbalance in the concentration of electrons and holes, which shifts the Shockley–Read–Hall (SRH) recombination statistics toward a slower rate.[41–43]

For all drive-in temperatures, after the hydrogenation treatment, the iV_{oc} is improved significantly, achieving an average iV_{oc} up to ≈700 mV for samples doped with <75% Ga. The samples doped with a 100% Ga solution show an even more dramatic increase, up to ≈720 mV. It is interesting to note here that the presence of B in the B + Ga doping solution limits the improvement of iV_{oc} after the hydrogenation. Such a limit does not apply, of course, to the 100% Ga samples, whose high iV_{oc} can be explained by the fact that, as chemical passivation is the dominant effect for them, there is more potential for the hydrogen to passivate the interfacial defects.

Figure 2B shows the contact resistivity (ρ_c) of the poly-Si/SiO_x passivating contacts spin-on doped with the various Ga + B solutions with different mixing ratios and annealed at different temperatures for 60 min, measured using the Cox and Strack method.[39] Increasing the drive-in temperature shows a decreasing contact resistivity, which is similar to the trend observed for other doping techniques.[44] With an annealing temperature of 1000 °C, a low contact resistivity of ≈4–60 $m\Omega\,cm^2$ can be achieved for different volume percentages of Ga in the doping solution. Meanwhile, increasing the volume percentage of Ga in the solution shows an increment in ρ_c. For the case of 100% Ga, the low annealing temperatures (900 and 930 °C) lead to very high contact resistivity values, which are beyond our measurement sensitivity. In fact, very high ρ_c values were also found

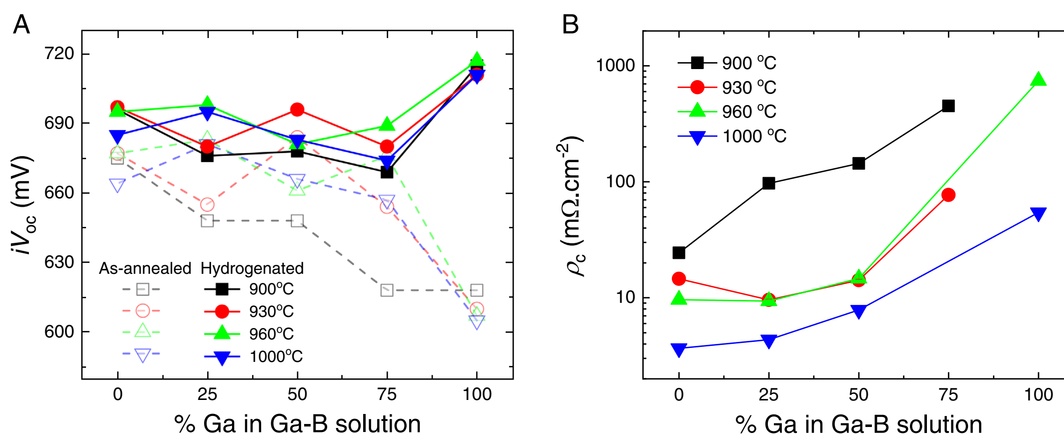

Figure 2. A) Implied open-circuit voltages iV_{oc} and B) contact resistivity ρ_c of various poly-Si/SiO_x/c-Si samples spin-doped by different volume percentages of Ga and B in the solution. The hydrogenation step was done by using a 20 nm-AlO_x/80 nm-SiN_x stack and forming gas annealing at 425 °C for 30 min.

© 2021 Wiley-VCH GmbH

2367198x, 2021, 12, Downloaded from https://onlinelibrary.wiley.com/doi/10.1002/solr.202100653 by The Australian National Univer, Wiley Online Library on [31/01/2023]. See the Terms and Conditions (https://onlinelibrary.wiley.com/terms-and-conditions) on Wiley Online Library for rules of use; OA articles are governed by the applicable Creative Commons License

in previous work using Ga for doping the poly-Si/SiO_x passivating contacts.[34] At high temperatures, ρ_c drops down from ≈800 mΩ cm^2 for 960 °C to 60 mΩ cm^2 for 1000 °C. Therefore, the low contact resistivity of 60 mΩ cm^2 at a high annealing temperature and the high iV_{oc} of ≈720 mV after hydrogenation achieved in this work are encouraging results for Ga-doped poly-Si contacts. For the cases with B present, comparing the results of iV_{oc} in Figure 2A and ρ_c in Figure 2B, we find that annealing the samples at a temperature of ≈930–960 °C shows relatively good passivating contact performance with sufficiently low ρ_c of ≈10 mΩ cm^2 and reasonably high iV_{oc} of up to ≈700 mV. Therefore, we choose 960 °C as the optimal annealing temperature for our subsequent characterization.

Next, we measure the doping profiles from the samples spin coated with different mixing ratios of Ga + B using the ECV and SIMS methods. With the ECV method, we can only detect the majority carrier concentration (holes in this case), which reflects the electrically active dopant concentration, regardless of the dopant type (B or Ga). Meanwhile, the SIMS concentration profiles account for all active and inactive dopant atoms, separately for each dopant type. **Figure 3**A,B shows the SIMS profiles of Ga and B, respectively, from 960 °C annealed samples for 60 min with various volume percentages of Ga in the mixed dopant solution. We note here that, in Figure 3A, for the 100% Ga samples, the Ga profile shows a surface error. This is likely due to the nature of the Ga spin-on doping with highly defective surfaces. Similar SIMS profiles of Ga-doped poly-Si samples have also been reported.[34] This also suggests that the location of the SiO_x interface in these samples is likely to have a large uncertainty. As can be seen from Figure 3A, increasing the percentage of Ga in the solution leads to a higher concentration of Ga in the poly-Si film and c-Si substrate. Generally, a base Ga profile with [Ga] of ≈1×10^{16} cm^{-3} can be seen on the 100% B profile. The Ga concentration in the poly-Si layer decreases significantly from the surface toward the SiO_x interface (as shown in Figure 3A). Meanwhile, for all the B profiles in Figure 3B, the concentrations of B in the poly-Si layer (≈5×10^{21} cm^{-3}), as well as in the c-Si substrate (except the 25%B sample), are similar. It indicates that the production of atomic Ga and B from their respective glass (oxides) is different. Also, it is evident that, in these poly-Si/SiO_x/Si structures, boron diffuses more deeply into the c-Si substrate than gallium (Figure 3B vs Figure 3A). This is probably due to a different blocking action of the thin SiO_x layer on each of the two dopant types, higher for Ga than for B. This is surprising, given that Ga has a six orders of magnitude higher diffusivity in SiO_x than B,[34] and it may be related to the fact that there are both Ga and B atoms in the glass layer and in the poly-Si film. For mixed solutions containing 50% Ga or less, very little Ga diffuses into the Si wafer; at the same time, B diffuses as deeply into the Si wafer for such mixed solutions as for the 100% B case. Only in the case of a 75% Ga + 25% B solution is the diffusion of B hindered to some extent by the presence of Ga in the Si wafer. Conversely, when there is any B present, it retards the diffusion of Ga.

In **Figure 4**, we visualize the inactive dopant concentrations of the different samples by plotting the SIMS and ECV profiles together. The inactive dopant concentrations are simply the difference between the sum of total dopant concentration profiles of Ga and B (by SIMS, solid curves), and the electrically active dopant profiles (by ECV, dashed curves). As can be seen from Figure 4, when the Ga volume percentage in the Ga + B solution is high (>50%), the electrically active dopant concentrations in the poly-Si layer as well as in the c-Si substrate decrease significantly. The 100% Ga-doped sample shows a very low active dopant profile (dashed black curve), immeasurably low near the surface of the poly-Si film, which agrees well with the surface result from the SIMS measurements (black curve, Figure 3A). Interestingly, even though there is a significant total concentration of Ga in the poly-Si layer, the concentration of electrically active Ga (i.e., functioning as acceptor atoms) is very low (≈2–3×10^{17} cm^{-3}). This explains the low surface passivation of the 100% Ga sample without hydrogenation, as shown in Figure 2A. Meanwhile, the combined total doping profiles (Ga + B) measured by SIMS in the poly-Si layer are similar across the different Ga:B ratios. The variation is more obvious as the dopants diffuse further into the substrate due to the different diffusivities of B and Ga in c-Si.

To better understand the amount of inactive dopants inside the stack of poly-Si/SiO_x/c-Si, integrated areas of the total SIMS curves and the ECV curves are calculated and compared. The resulting percentages of active and inactive dopants in

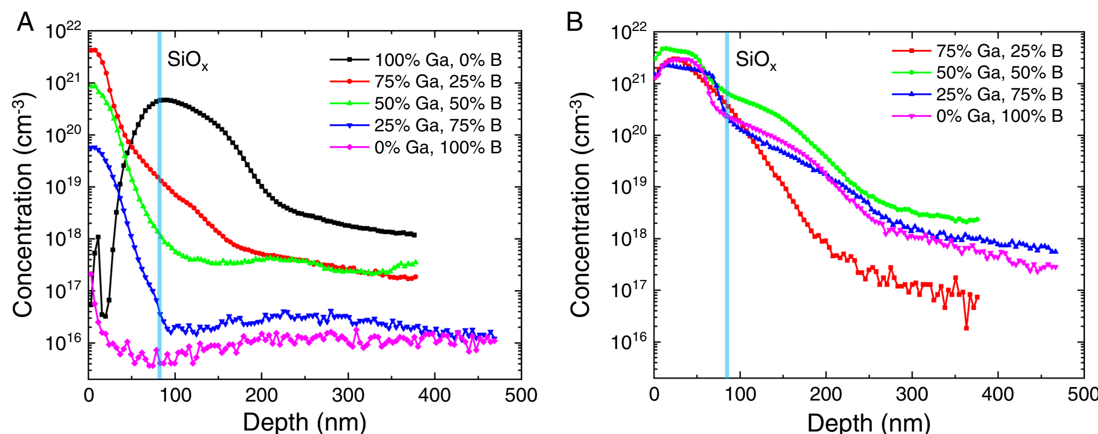

Figure 3. SIMS depth profiles for A) Ga and B) B for spin-on-doped poly-Si/SiO_x passivating contacts after a 960 °C, 60 min anneal with different Ga volume percentages in the Ga–B solution.

© 2021 Wiley-VCH GmbH

2367198x, 2021, 12, Downloaded from https://onlinelibrary.wiley.com/doi/10.1002/solr.202100653 by The Australian National Univer, Wiley Online Library on [31/01/2023]. See the Terms and Conditions (https://onlinelibrary.wiley.com/terms-and-conditions) on Wiley Online Library for rules of use; OA articles are governed by the applicable Creative Commons License

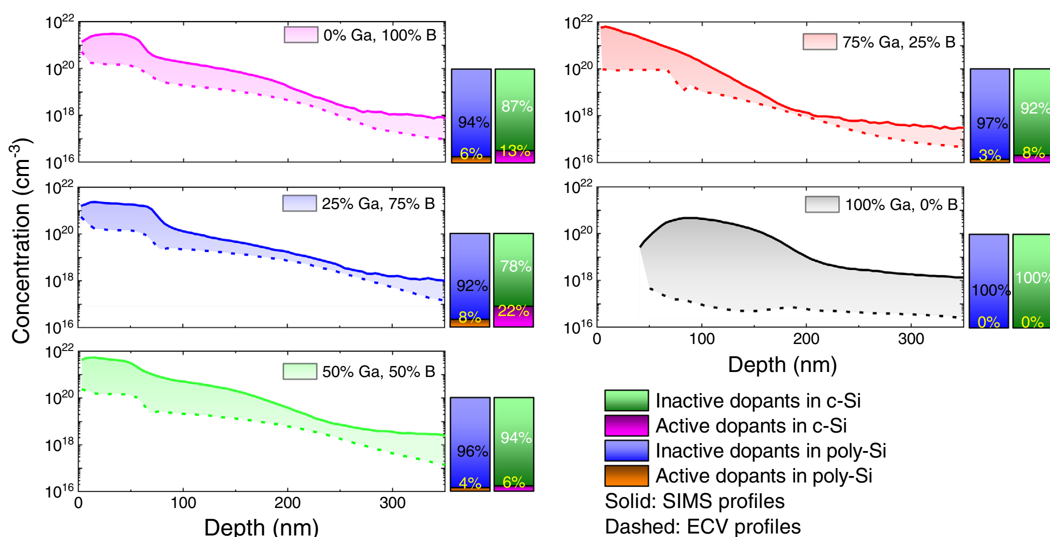

Figure 4. Total doping profiles by SIMS for Ga and B (solid lines) and their corresponding electrically active doping profiles by ECV (dashed lines). Percentages of active and inactive dopants in the poly-Si and c-Si, respectively, calculated by integrating the area between the SIMS and ECV profiles, were plotted as the insets beside the doping profiles.

poly-Si and c-Si are shown in the insets of Figure 4. The integration ranges are 0–80 nm (SiO_x location) and 80–350 nm for the poly-Si layer and c-Si substrate, respectively. Note here that, due to the measurement errors at the surface, for the 100% Ga sample an integration range from 50 to 80 nm was chosen for the poly-Si layer. Overall, for all mixed volume percentages of Ga in the Ga + B solution, the concentration of inactive dopants (both Ga and B) in the c-Si wafer is significantly higher than the concentration of electrically active dopants (Figure 4 insets, green vs magenta columns). The ratio between inactive to total dopant concentration is even higher in the poly-Si layer (>80%, blue columns). Generally, a higher Ga volume percentage in the Ga + B solution causes an increased amount of inactive dopants in both the c-Si substrate and the poly-Si layer (green columns, Figure 4).

The in-diffusion of dopants into the substrate causes, in principle, Auger recombination in the diffused layer underneath the oxide. Nevertheless, this only applies to the electrically active dopant profile, which is quite moderate for all the samples in Figure 4, with a maximum concentration of $2–3 \times 10^{19}$ cm^{-3}. More concerning is the presence of a significant amount of inactive dopants, mostly B, in that diffused layer. It is likely that those inactive dopants create recombination centers, and therefore they can be a contributing factor for the relatively modest iV_{oc} measured for most samples in Figure 2A.[45,46] The sample with 100% Ga and no B behaves differently because despite most of the Ga being inactive, it shows the highest iV_{oc}. This would indicate that the presence of inactive Ga is not as harmful as that of inactive B.

4. Conclusions

In conclusion, we have fabricated and investigated p-type poly-Si/SiO_x passivating contacts using the spin-on doping method with Ga + B mixture solutions as the dopant sources. The effects of Ga mixing volume percentage in the Ga + B solutions on the performance and optoelectronic properties of the passivating contacts were studied. It was found that independent of the Ga:B volume ratio, the surface passivation after the hydrogenation treatment of AlO_x/SiN_x + FGA was improved, reaching $iV_{oc} > 700$ mV. Using ECV and SIMS doping profiles, the percentages of inactive and active dopants inside the poly-Si films and c-Si substrates were calculated and compared. It was found that, even though a high concentration of Ga was diffused into the poly-Si and c-Si, the amount of active dopants remained low. These findings on the behaviors of B and Ga codoping may help to optimize p-type poly-Si passivating contacts for Si solar cells.

Acknowledgements

This work has been supported by the Australian Renewable Energy Agency (ARENA) through projects RND016 and RND017. The authors acknowledge access to equipment at the Australian National Fabrication Facility (ANFF), ACT Node, and the Department of Electronic Materials Engineering, The Australian National University. H.T.N. and J.S. acknowledge fellowship support from the Australian Centre for Advanced Photovoltaics (ACAP).

Conflict of Interest

The authors declare no conflict of interest.

Data Availability Statement

The data that support the findings of this study are available from the corresponding authors upon reasonable request.

Keywords

boron, gallium, passivating contacts, POLO, poly-Si, spin-on doping, TOPCon

© 2021 Wiley-VCH GmbH

Received: August 17, 2021
Revised: October 8, 2021
Published online: October 24, 2021

[1] M. A. Green, *Joule* **2019**, *3*, 631.
[2] M. A. Green, *Nat. Rev. Phys.* **2020**, *2*, 172.
[3] M. A. Green, *Prog. Energy* **2019**, *1*, 013001.
[4] M. Hermle, F. Feldmann, M. Bivour, J. C. Goldschmidt, S. W. Glunz, *Appl. Phys. Rev.* **2020**, *7*, 021305.
[5] T. G. Allen, J. Bullock, X. Yang, A. Javey, S. De Wolf, *Nat. Energy* **2019**, *4*, 914.
[6] E. Bellini, *Longi achieves 25.21% efficiency for TOPCon solar cell,* **2021** https://www.pv-magazine.com/2021/06/02/longi-achieves-25-21-efficiency-for-topcon-solar-cell-announces-two-more-records/, n.d.
[7] S. Hamma, P. Cabarrocas, *Sol. Energy Mater. Sol. Cells* **2001**, *69*, 217.
[8] F. Feldmann, M. Simon, M. Bivour, C. Reichel, M. Hermle, S. W. Glunz, *Appl. Phys. Lett.* **2014**, *104*, 181105.
[9] J. Stuckelberger, G. Nogay, P. Wyss, Q. Jeangros, C. Allebé, F. Debrot, X. Niquille, M. Ledinsky, A. Fejfar, M. Despeisse, F. J. Haug, P. Löper, C. Ballif, *Sol. Energy Mater. Sol. Cells* **2016**, *158*, 2.
[10] B. Nemeth, D. L. Young, M. R. Page, V. Lasalvia, S. Johnston, R. Reedy, P. Stradins, *J. Mater. Res.* **2016**, *31*, 671.
[11] Y. Larionova, M. Turcu, S. Reiter, R. Brendel, D. Tetzlaff, J. Krügener, T. Wietler, U. Höhne, J. D. Kähler, R. Peibst, *Phys. Status Solidi Appl. Mater. Sci.* **2017**, *214*, 1700058 https://doi.org/10.1002/pssa.201700058.
[12] D. Yan, A. Cuevas, S. P. Phang, Y. Wan, D. Macdonald, *Appl. Phys. Lett.* **2018**, *113*, 061603.
[13] H. Tong, M. Liao, Z. Zhang, Y. Wan, D. Wang, C. Quan, L. Cai, P. Gao, W. Guo, H. Lin, C. Shou, Y. Zeng, B. Yan, J. Ye, *Sol. Energy Mater. Sol. Cells* **2018**, *188*, 149.
[14] A. Ingenito, G. Nogay, Q. Jeangros, E. Rucavado, C. Allebé, S. Eswara, N. Valle, T. Wirtz, J. Horzel, T. Koida, M. Morales-Masis, M. Despeisse, F. J. Haug, P. Löper, C. Ballif, *Nat. Energy* **2018**, *3*, 800.
[15] Z. Wang, Z. Liu, M. Liao, D. Huang, X. Guo, Z. Rui, Q. Yang, W. Guo, J. Sheng, C. Shou, B. Yan, Z. Yuan, Y. Zeng, J. Ye, *Sol. Energy Mater. Sol. Cells* **2020**, *206*, 110256.
[16] S. Ingole, P. Aella, P. Manandhar, S. B. Chikkannanavar, E. A. Akhadov, D. J. Smith, S. T. Picraux, *J. Appl. Phys.* **2008**, *103*, 104302 https://doi.org/10.1063/1.2924415.
[17] F. Feldmann, R. Müller, C. Reichel, M. Hermle, *Phys. Status Solidi RRL* **2014**, *8*, 767.
[18] R. Peibst, U. Romer, Y. Larionova, H. Schulte-Huxel, T. Ohrdes, M. Haberle, B. Lim, J. Krugener, D. Stichtenoth, T. Wutherich, C. Schollhorn, J. Graff, R. Brendel, *2014 IEEE 40th Photovolt. Spec. Conf. PVSC*, IEEE, Piscataway, NJ **2014**, p. 852.
[19] D. Yan, A. Cuevas, J. Bullock, Y. Wan, C. Samundsett, *Sol. Energy Mater. Sol. Cells* **2015**, *142*, 75.
[20] C. Reichel, F. Feldmann, R. Müller, R. C. Reedy, B. G. Lee, D. L. Young, P. Stradins, M. Hermle, S. W. Glunz, *J. Appl. Phys.* **2015**, *118*, 205701 https://doi.org/10.1063/1.4936223.
[21] M. K. Stodolny, M. Lenes, Y. Wu, G. J. M. Janssen, I. G. Romijn, J. R. M. Luchies, L. J. Geerligs, *Sol. Energy Mater. Sol. Cells* **2016**, *158*, 24.
[22] J. Krügener, F. Haase, M. Rienäcker, R. Brendel, H. J. Osten, R. Peibst, *Sol. Energy Mater. Sol. Cells* **2017**, *173*, 85.
[23] F. Feldmann, C. Reichel, R. Müller, M. Hermle, *Sol. Energy Mater. Sol. Cells* **2017**, *159*, 265.
[24] S. Duttagupta, N. Nandakumar, P. Padhamnath, J. K. Buatis, R. Stangl, A. G. Aberle, *Sol. Energy Mater. Sol. Cells* **2018**, *187*, 76.
[25] G. S. May, S. M. Sze, *Fundamentals of Semiconductor Fabrication*, Wiley, New Jersey **2015**.
[26] Z. Ding, T. N. Truong, H. T. Nguyen, D. Yan, X. Zhang, J. Yang, Z. Wang, P. Zheng, Y. Wan, D. Macdonald, J. Stuckelberger, *ACS Appl. Energy Mater.* **2021**, *4*, 4993.
[27] X. Yang, J. Kang, W. Liu, X. Zhang, S. De Wolf, *ACS Appl. Mater. Interfaces* **2021**, *13*, 8455.
[28] F. Bensebaa, in *Interface Science and Technology*, Elsevier, Amsterdam. Vol. *19*, **2013**, pp. 185–277.
[29] Z. Kiaee, C. Reichel, Z. Hussain, M. Nazarzadeh, J. D. Huyeng, F. Clement, M. Hermle, R. Keding, *Sol. Energy Mater. Sol. Cells* **2021**, *222*, 110926.
[30] T. E. Hawkinson, D. B. Korpela, in *Semiconductor Safety Handbook*, Elsevier, Amsterdam NY **1998**, pp. 187–203.
[31] H. Ryssel, K. Haberger, in *Ion Implantation: Science and Technology*, Elsevier, Amsterdam NY **1984**, pp. 603–627.
[32] S. M. Sze, K. K. Ng, *Physics of Semiconductor Devices*, John Wiley & Sons, Inc., Hoboken, NJ, **2006**.
[33] M. Forster, E. Fourmond, R. Einhaus, H. Lauvray, J. Kraiem, M. Lemiti, *Phys. Status Solidi C* **2011**, *8*, 678.
[34] D. L. Young, B. G. Lee, D. Fogel, W. Nemeth, V. LaSalvia, S. Theingi, M. Page, M. Young, C. Perkins, P. Stradins, *IEEE J. Photovoltaics* **2017**, *7*, 1640.
[35] S. W. Glunz, S. Rein, J. Knobloch, W. Wettling, T. Abe, *Prog. Photovoltaics Res. Appl.* **1999**, *7*, 463.
[36] C. M. Lin, A. J. Steckl, T. P. Chow, *IEEE Electron Device Lett.* **1988**, *9*, 594.
[37] A. S. Grove, O. Leistiko, C. T. Sah, *J. Phys. Chem. Solids* **1964**, *25*, 985.
[38] R. N. Linnebach, *J. Appl. Phys.* **1990**, *67*, 6794.
[39] R. H. Cox, H. Strack, *Solid. State. Electron.* **1967**, *10*, 1213.
[40] C. Hollemann, N. Folchert, S. P. Harvey, P. Stradins, D. L. Young, C. L. Salles de Souza, M. Rienäcker, F. Haase, R. Brendel, R. Peibst, *Sol. Energy Mater. Sol. Cells* **2021**, *231*, 111297.
[41] P. Würfel, *Physics of Solar Cells*, Wiley, New York **2005**.
[42] U. Wurfel, A. Cuevas, P. Wurfel, *IEEE J. Photovoltaics* **2015**, *5*, 461.
[43] A. Cuevas, Y. Wan, D. Yan, C. Samundsett, T. Allen, X. Zhang, J. Cui, J. Bullock, *Sol. Energy Mater. Sol. Cells* **2018**, *184*, 38.
[44] F. Feldmann, M. Bivour, C. Reichel, M. Hermle, S. W. Glunz, *Sol. Energy Mater. Sol. Cells* **2014**, *120*, 270.
[45] U. Römer, R. Peibst, T. Ohrdes, B. Lim, J. Krügener, E. Bugiel, T. Wietler, R. Brendel, *Sol. Energy Mater. Sol. Cells* **2014**, *131*, 85.
[46] R. Peibst, U. Römer, Y. Larionova, M. Rienäcker, A. Merkle, N. Folchert, S. Reiter, M. Turcu, B. Min, J. Krügener, D. Tetzlaff, E. Bugiel, T. Wietler, R. Brendel, *Sol. Energy Mater. Sol. Cells* **2016**, *158*, 60.

© 2021 Wiley-VCH GmbH

2367198x, 2021, 12, Downloaded from https://onlinelibrary.wiley.com/doi/10.1002/solr.202100653 by The Australian National Univer, Wiley Online Library on [31/01/2023]. See the Terms and Conditions (https://onlinelibrary.wiley.com/terms-and-conditions) on Wiley Online Library for rules of use; OA articles are governed by the applicable Creative Commons License